Laser printing of optically resonant hollow crystalline carbon nanostructures from 1D and 2D metal–organic frameworks

Leila Mingabudinova, Anastasiia Zalogina, Andrei Krasilin, Margarita Petrova, Pavel Trofimov, Yuri Mezenov, Evgeniy Ubyivovk, Peter Lönnecke, Alexandre Nomine, Jaafar Ghanbaja, et al.

Laser printing of optically resonant hollow crystalline carbon nanostructures from 1D and 2D metal–organic frameworks

Leila R. Mingabudinova,[a] Anastasiia S. Zalogina,[b] Andrei A. Krasilin,[b] Margarita I. Petrova,[b] Pavel Trofimov,[b] Yuri A. Mezenov,[b] Evgeniy V. Ubyivovk,[c] Peter Lönnecke,[d] Alexandre Nominé,[b] Jaafar Ghanbaja,[e] Thierry Belmonte,[e] and Valentin A. Milichko

[a] Physics and Chemistry of Nanostructures Group, Ghent University, B-9000 Gent, Belgium

[b] Department of Nanophotonics and Metamaterials, ITMO University, St. Petersburg, 197101, Russia.

[c] St. Petersburg State University, St. Petersburg 199034, Russia

[d] Institut für Anorganische Chemie, Universität Leipzig, 04103 Leipzig, Germany

[e] Université de Lorraine, Institut Jean Lamour, UMR CNRS 7198, Nancy F-54011, France

ABSTRACT

Using a hybrid approach involving a slow diffusion method to synthesize 1D and 2D MOFs followed by their treatment with femtosecond infrared laser radiation, we generated 100–600 nm well-defined hollow spheres and hemispheres of graphite. This ultrafast technique extends the library of shapes of crystalline MOF derivatives appropriate for all-dielectric nanophotonics.

Owing to the synergistic combination of organic and inorganic building blocks providing chemically active nanoporous structures with exceptional mechanics,[1] metal–organic frameworks are establishing their position as an important class of highly versatile and tuneable crystalline materials for diverse applications.[2–4] Their unconventional property of softness provides provides the structural changes under different stimuli such as pressure, temperature, electric and magnetic fields and light.[4–6] Utilizing these stimuli at an extreme regime (high temperatures, strong electric fields, etc.) yields the MOF structure transformation to the amorphous phase[7] and then to the derivative compound:8–10 amorphous carbon nanostructures, nanocrystalline graphite, metal oxides, chalcogenides, phosphides, carbides and pure metallic nanoclusters. Utilizing MOFs as precursors for the fabrication of nanoparticles with a regular structure (e.g., graphite) and complex shape (hollow spheres, cubes, yolk–shell, etc.) is essential due to key reasons: the MOF crystal itself represents the template for its derivatives with well-defined shapes;[8–10] the relatively high temperature stability of MOFs allows their transformation to derivatives avoiding the thermal decomposition of pure organic components prior to completion of the transformation process;[8] and finally, the regular structure of MOFs yields a uniform distribution and ordering of carbon which is not possible by simple mixing of the carbon precursors.[10] However, the existing techniques for fabrication of the MOF derivatives are slow (from tens of minutes to hours) and energy expensive, as well as the limited number of derivative types and shapes constrain the fields of their application by energy storage[9–11] and catalysis.[12] On the other hand, the wide variety of complex topologies and mesoscale architectures available among the several hundreds of chained (1D) and layered (2D) MOFs reported so far (see the Cambridge Crystallographic Data Centre) renders these materials unique starting points for fabricating previously implausible nanostructures for nanophotonics and light manipulation.

Here we report a general top-down strategy that enables the fabrication of a new type of MOF derivatives for all-dielectric nanophotonics,[13] – nanometer-scale well-defined hollow spheres and hemispheres, whose shells are crystalline carbon (graphite). We utilize MOFs synthesized via reticular chemistry[14] as the template material. We then investigate for the first time the use of infrared femtosecond laser pulses as the means for providing the external stimulus necessary for reassembling the complex structure of MOF single crystals into three-dimensional (3D) crystalline hollow carbon structures (c-HCS). The structures obtained have diameters ranging from 100 to 600 nm and demonstrate the resonant light–matter interaction – the polarization-dependent scattering of light due to the generation of specific Mie-type modes.

At first, the bulk 1D MOF crystalline precursors were synthesized by a slow diffusion method following a modified procedure[15] (for details, see ESI) that allows controlled growth of the coordination polymer from a bidentate 1,2-di(4-pyridyl) ethylene (BPE) ligand and $Cu(NO_3)_2 \cdot 6(H_2O)$

metal precursor. In a typical experiment, the solutions of the copper salt and the BPE ligand in dimethylformamide (DMF) were brought together under the slow diffusion conditions at room temperature in the course of one week. Single crystal X-ray diffraction analysis on the obtained material with the brutto formula of $[Cu(C_{12}H_{10}N_2)(NO_3)_2]\cdot DMF\cdot i\text{-}PrOH$ (1) revealed a triclinic crystal system with $P1^-$ symmetry (Fig. 1A, and ESI, Fig. S1, S2, Table S1) featuring dimeric threads composed of the octahedral copper dimers held together by μ-O bridges from the nitrate ligands occupying the equatorial position of the Cu sites. The axial sites are occupied by the BPE ligands establishing two parallel threads of aromatic moieties. These threads are stacked together into van der Waals layers (Fig. 1A) with DMF and i-PrOH molecules confined between them.

Secondly, we synthesized alternative 2D MOF (2) with a more rigid tetradentate BPY ligand having the brutto formula of $[Cu(bipy)2(DMF)(NO_3)][NO_3]\cdot 3DMF$, a monoclinic crystal system with the P_{21}/n space group and layered van der Waals structure (ESI, Tables S2–S6 and Fig. S13).

We then generated c-HCSs from the single crystals of 1 and 2 (Fig. 1B) by adopting a laser method (see the scheme in ESI, Fig. S3) previously used to synthesize the crystalline bulk[16] and, in some case, hollow[17] pure inorganic nanostructures (silicon or metal oxides). Here, individual MOF crystals placed on a fused silica substrate in air were exposed to 150 femtosecond 1050 nm laser pulses with 80 MHz repetition rate and 5 W maximal power focused by a 10× 0.28NA objective (Fig. 1C). By varying the power from 60 to 160 mW using an interference filter, we were able to burst single crystals (Fig. 1D). The nanostructures produced were visualized using dark field microscopy (Fig. 1E). The irradiation at a low power (<100 mW) resulted in the simple cutting of MOFs, whereas the higher power (100 to 120 mW) allowed to the full conversion of MOF to nanostructures (Fig. 2A and B). Increasing the power to hundreds of milliwatts yielded the transformation of MOFs to a “carpet” of fused organic–inorganic compounds without any intriguing structures. It should also be noted that the light-induced conversion of MOF single crystals into nanostructures was extremely fast. The characteristic times for the process in our case was of the order of microseconds or faster (up to nanoseconds) similar to the timescales of the related transformations of inorganic nanocrystallites.[16]

The generated nanostructures were then transferred onto a fused silica substrate, gold film or carbon grid for a detailed characterization using electron and optical microscopy. At first, scanning electron microscopy (SEM, Carl Zeiss, Neon 40) was used to analyse the impact of the varying laser intensity on the average shape and size of nanostructures obtained. For compound 1, our procedure mainly led to the formation of spheres (Fig. 2C and D) and, to a lesser extent, to shapeless structures with diameters ranging from 20 to 600 nm (Fig. 2A). The smallest structures with diameters of 20–80

nm were formed at laser powers from 60 to 160 mW, whereas the larger ones were only obtained under irradiation with 100–120 mW (Fig. 2A). For compound 2, we observed mostly the hemispheres (ESI, Fig. S14) with the diameter ranging from 200 to 600 nm and, to a lesser extent, shapeless structures of 20–100 nm in diameter.

Inspired by the recent findings[18–20] that specific information about the structure of complex materials such as MOFs could be directly extracted from the results of Transmission Electron Microscopy (TEM), we used this to provide insights into the structural and composition properties of the nanostructures obtained. TEM (JEOL ARM 200F Cold FEG TEM/STEM operating at 200 kV) reveals that they have different shapes, from hollow spheres to hemispheres (Fig. 2F–I, and ESI, Fig. S4, 5, 14) depending on the initial MOF structure. The shell thickness is inversely proportional to the total diameter and varies from 1/12 and 1/3 of the total diameter (ESI, Fig. S5). High-resolution TEM micrographs (Fig. 2K, L, 3A, B, and ESI, Fig. S10) reveal a thin amorphous layer on the outer side and a thicker perfectly crystallized shell. The fast Fourier transform (FFT) analysis of the crystalline shell (Fig. 3C, ESI, S10) shows a 2-fold symmetry pattern with typical interplanar distance dhkl equal to 3.3 ± 0.1 Å being in a good agreement with previous results on hollow carbon spheres (graphite).[21–27] This measurement is supported by the direct intensity histogram that reveals a period of 3.39 ± 0.10 Å (ESI, Fig. S10). The energy dispersive X-ray analysis, EDX, (Fig. 3D–F) also demonstrates the carbon nature of c-HCS since oxygen and nitrogen are detected only on the surface in small amounts. One can conclude that c-HCSs obtained are actually composed of graphite that presents a structure of pure carbon layers with theoretical interplanar distances of 3.35 Å for the (002) plane. It should be noted that during the laser treatment the copper ions should also undergo the transformation into oxides, carbides, etc.[8–10] Using TEM we also observed a small amount of amorphous metal–organic nanoparticles7 with nanometer scale inclusions (ESI, Fig. S11), which were characterized by high electron density.[12] This is explained by the presence of copper in the composition (see the EDX map in the ESI, Fig. S12). Moreover, depending on the time elapsed between the MOF synthesis and its laser treatment, the number of copper-based nanostructures increases, while the number of c-HCSs dramatically decreases indicating the negative effect of the degradation of MOF structure on the c-HCS fabrication.

The dependence of the shape of c-HCS obtained (sphere or hemisphere) directly correlates with the topology of initial MOFs (chained or layered). The fast transformation of the dimeric MOF threads (1) into crystal carbon spheres can be governed by the high mobility of the van der Waals layers and substantial elasticity of their hybrid covalent–ionic structural domains that allows them to arrange into an energetically favourable spherical shape (ESI, Fig. S6). Indeed, the similar 2D MOF (2) with a more rigid tetradentate BPY ligand having a layered van der Waals structure yielded well-

defined crystalline hemispheres under the same stimuli. This supports that 1D and 2D MOFs with flexible and/or quite rigid layered structure are suitable for ultra-fast transformation to complete 3D nanostructures with a regular topology. To confirm this we also applied the developed laser-assisted technique for other MOFs as template materials: we utilized rigid 3D microcrystals based on zinc and cadmium ions.[28] Surprisingly, the yield of c-HCS was dramatically small (less than 1% of all fabricated nanostructures) arguing that flexible 1D and 2D crystalline metal– organic frameworks with weak inter-layer and inter-chain interactions are more suitable for the assembly of graphite nanostructures with unique well-defined shapes such as hollow spheres and hemispheres.

In contrast to existing MOF derivatives,[8–10] our study extends their library of shapes. Moreover, compared to previously reported 20–300 nm and micrometre-size hollow graphite spheres,[24] our laser-assisted technique provides the fastest and non-equilibrium strategy to create c-HCSs in air with extended diameters ranging from 100 to 600 nm. In addition, this technique allows us to achieve a relatively high yield of the product (Fig. 2A and B). Statistical data obtained from the complex of SEM and TEM analyses proves that up to 40% of all the nanostructured produced are c-HCSs, and the remaining 60% are amorphous nanoparticles and nanometre to micrometre shards of MOFs. Besides the conventional application of carbon structures in energy storage,[9,10] the current 3D structures hold a great potential for all-dielectric nanophotonics,[13,29] where the functional elements should strictly fulfill the following requirements: (i) a high refractive index necessary for a sufficient optical contrast with an ambient medium (air), (ii) specific shape to enable the generation of different optical modes as well as (iii) perfect crystallinity to suppress non-radiative decay of light energy at optical resonances. Indeed, crystalline carbon (graphite) has a relatively high refractive index of 2.6–3.0 within the whole visible range.[30] The optical characterization of single c-HCSs in dark field geometry with polarization resolution was performed with a commercial confocal spectrometer, Horiba LabRam (Fig. 3G, H and ESI, S3). The measurements revealed the colour selectivity in scattering from the blue to red regions of the visible range, depending on the light polarization. This can be explained by the generation of different optical modes (Mie-type) inside the spheres (ESI, Fig. S16). Intriguingly, due to the hollow shape of c-HCSs, the electric field of the magnetic Mie-type modes should be localized inside the shell,[13] while the magnetic part of light is concentrated in a cavity. Such a behaviour can only be manifested in hollow nanostructures and may find optical and even medical application. Previously such an effect has only been observed for all-dielectric silicon cylinders[31] rendering the current c-HCSs as the first example of a magnetic resonant structure being easy to be fabricated. This provides a unique opportunity for the enhancement and efficient interaction of the magnetic component of light with matter inside the cavity.

In summary, we demonstrate an ultra-fast laser-assisted technique to fabricate new types of MOF derivatives – 100–600 nm well-defined hollow spheres and hemispheres, whose shells are crystalline carbon (graphite). This technique overcomes the requirements of specific gas atmosphere, additional precursors and high-energy consumption to heat the compound; this significantly simplifies the synthesis which is important for real-world application. Intriguingly, the technique also allows us to extend the library of shapes and size of crystalline MOF derivatives. The nanostructures obtained possess unique shapes and crystallinities, and consequently demonstrate polarization-dependent light scattering due to the generation of different optical modes inside important for all-dielectric nanophotonics and light manipulation.

Acknowledgements

The authors wish to thank Prof. E. A. Pidko (TU Delft) for fruitful discussions, Dr S. A. Sapchenko (Nikolaev Institute of Inorganic Chemistry) for kindly providing rigid 3D MOFs, Dr A. V. Vinogradov (ITMO University) for support in reticular synthesis, Prof. Kristof Van Hecke (Ghent University) for crystallographic support, Dr D. A. Zuev (ITMO University) for assistance in laser ablation, Dr S. V. Makarov (ITMO University) for discussion on optical scattering, and F. E. Komissarenko (ITMO University) for preliminary SEM analysis. This work is a part of a joint Russian-French project “Hybrid photonics nanodevices” and is supported by the Ministry of Science and Higher Education of the Russian Federation (project No 14.587.21.0050 with unique identification RFMEFI58718X0050). ITMO University is acknowledged for providing access to the unique scientific instruments (AIST-NT TrIOS) for optical experiments.

Notes and references

1 S. Horike, S. Shimomura and S. Kitagawa, Nat. Chem., 2009, 1, 695–704.

2 H. Furukawa, U. Muller and O. M. Yaghi, Angew. Chem., Int. Ed., 2015, 54, 3417–3430.

3 N. C. Burtch, J. Heinen, T. D. Bennett, D. Dubbeldam and M. D. Allendorf, Adv. Mater., 2018, 30, 1704124.

4 V. A. Milichko, S. V. Makarov, A. V. Yulin, A. V. Vinogradov, A. A. Krasilin, E. Ushakova, V. P. Dzyuba, E. Hey-Hawkins, E. A. Pidko and P. A. Belov, Adv. Mater., 2017, 29, 1606034.

5 O. Sato, Nat. Chem., 2016, 8, 644–656.

6 F. X. Coudert, Chem. Mater., 2015, 27, 1905–1916.

7 R. Gaillac, P. Pullumbi, K. A. Beyer, K. W. Chapman, D. A. Keen, T. D. Bennett and F. X. Coudert, Nat. Mater., 2017, 16, 1149–1154.

8 Y. V. Kaneti, J. Tang, R. R. Salunkhe, X. Jiang, A. Yu, K. C. W. Wu and Y. Yamauchi, Adv. Mater., 2017, 29, 1604898.

9 B. Y. Guan, X. Y. Yu, H. B. Wu and X. W. Lou, Adv. Mater., 2017, 29, 1703614.

10 A. Indra, T. Song and U. Paik, Adv. Mater., 2018, 30, 1705146.

11 M. H. Yap, K. L. Fow and G. Z. Chen, Green Energy Environ., 2017, 2, 218–245.

12 R. V. Jagadeesh, L. Murugesan, A. S. Alshammari, H. Neumann, M. M. Pohl, J. Radnik and M. Beller, Science, 2017, 358, 326–332.

13 A. I. Kuznetsov, A. E. Miroshnichenko, M. L. Brongersma, Y. S. Kivshar and B. Luk'yanchuk, Science, 2016, 354, aag2472.

14 O. M. Yaghi, M. O'Keeffe, N. W. Ockwig, H. K. Chae, M. Eddaoudi and J. Kim, Nature, 2003, 423, 705–714.

15 A. V. Vinogradov, H. Zaake-Hertling, A. S. Drozdov, P. Lönnecke, J. A. Seisenbaeva, V. G. Kessler, V. V. Vinogradov and E. Hey-Hawkins, Chem. Commun., 2015, 51, 17764–17767.

16 P. A. Dmitriev, S. V. Makarov, V. A. Milichko, I. S. Mukhin, A. S. Gudovskikh, A. A. Sitnikova, A. K. Samusev, A. E. Krasnok and P. A. Belov, Nanoscale, 2016, 8, 5043–5048.

17 H. Yu, X. Li, Y. Zhu, Z. Hao and X. J. Zeng, J. Phys. Chem. C, 2017, 121, 12469–12475.

18 Y. Zhu, J. Ciston, B. Zheng, X. Miao, C. Czarnik, Y. Pan, R. Sougrat, Z. Lai, C. E. Hsiung, K. Yao, I. Pinnau, M. Pan and Y. Han, Nat. Mater., 2017, 16, 532–536.

19 D. Zhang, Y. Zhu, L. Liu, X. Ying, C. E. Hsiung, R. Sougrat, K. Li and Y. Han, Science, 2018, 359, 675–679.

20 T. Ma, E. A. Kapustin, S. X. Yin, L. Liang, Z. Zhou, J. Niu, L. H. Li, Y. Wang, J. Su, J. Li, X. Wang, W. D. Wang, W. Wang, J. Sun and O. M. Yaghi, Science, 2018, 361, 48–52.

21 G. Zou, D. Yu, J. Lu, D. Wang, C. Juang and Y. A. Qian, Solid State Commun., 2004, 131, 749–752.

22 F. D. Han, Y. J. Bai, R. Liu, B. Yao, Y. X. Qi, N. Lun and J. X. Zhang, Adv. Energy Mater., 2011, 1, 798–801.

23 J. Kang, O. L. Li and N. Saito, Carbon, 2013, 60, 292– 298.

24 J. Liu, N. P. Wickramaratne, X. Z. Qiao and M. Jaroniec, Nat. Mater., 2015, 14, 763–774.

25 K. Tang, R. J. White, X. Mu, M. M. Titirici, P. A. van Aken and J. Maier, ChemSusChem, 2012, 5, 400–403.

26 Z. S. Wang and F. S. Li, Mater. Lett., 2009, 63, 58–60. 27 W. Zhang, X. Jiang, Y. Zhao, A. Carne-Sanchez, V. Malgras, J. Kim, J. H. Kim, S. Wang, J. Liu, J. S. Jiang, Y. Yamauchi and M. Hu, Chem. Sci., 2017, 8, 3538–3546.

28 M. O. Barsukova, S. A. Sapchenko, K. A. Kovalenko, D. G. Samsonenko, A. S. Potapov, D. N. Dybtsev and V. P. Fedin, New J. Chem., 2018, 42, 6408–6415.

29 S. V. Makarov, A. N. Tsypkin, T. A. Voytova, V. A. Milichko, I. S. Mukhin, A. V. Yulin, S. E. Putilin, M. A. Baranov, A. E. Krasnok, I. A. Morozov and P. A. Belov, Nanoscale, 2016, 8, 17809–17814.

30 A. B. Djurišić and E. H. Li, J. Appl. Phys., 1999, 85, 7404–7410.

31 M. A. van der Haar, J. van de Groep, B. J. M. Brenny and A. Polman, Opt. Express, 2016, 24, 2047.

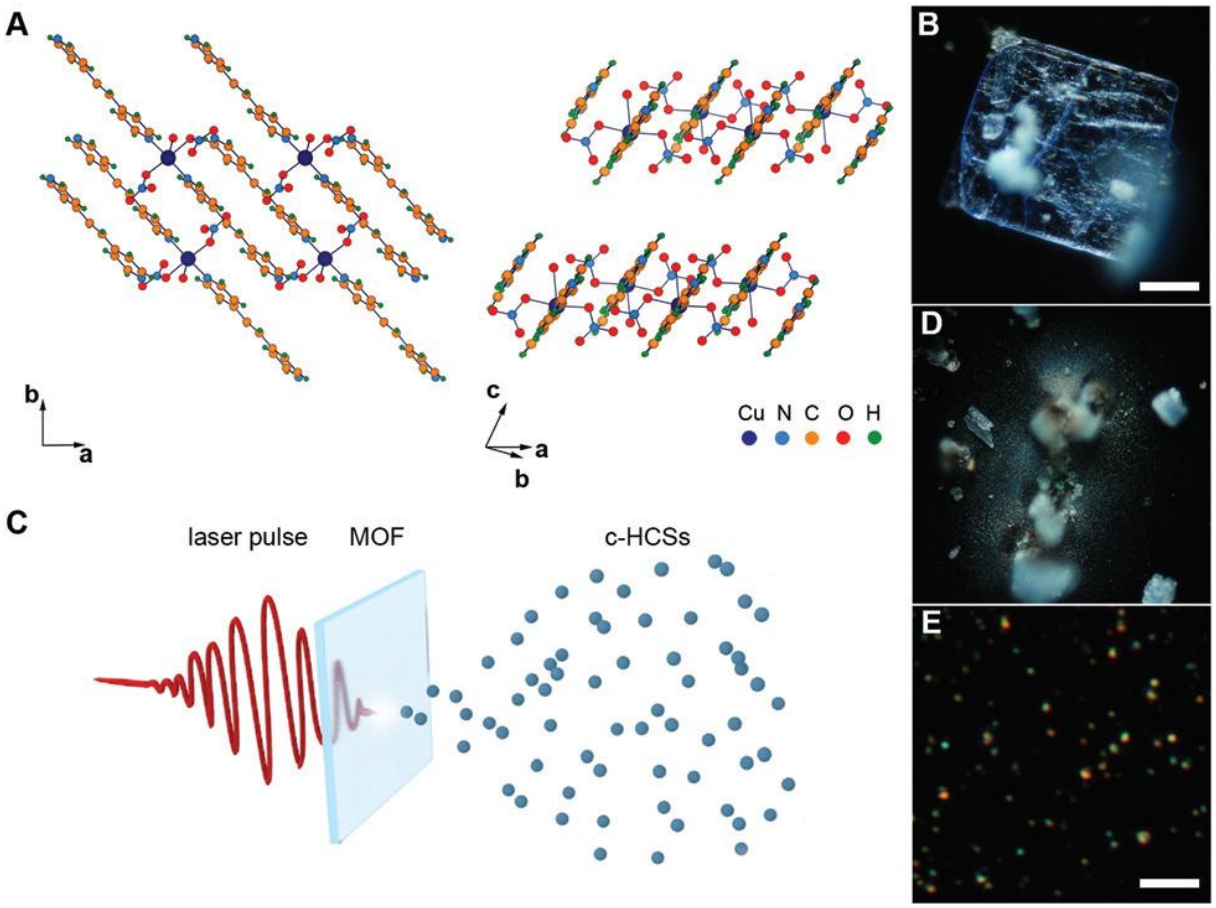

Fig. 1: Laser-assisted synthesis of c-HCS. (A) Crystal structure of Cubased MOF (1) along different axes. The crystal has a triclinic structure with $P1^{-}$ symmetry featuring dimeric chains stacked together into a van der Waals layered structure with DMF and i-PrOH molecules confined between the layers (not shown here). (B) Dark field optical image of single crystals of 1. Scale bar, 5 µm. (C) Exposure of the MOF single crystal to 150 fs infrared laser pulses in air produces nanostructures (c-HCSs). (D) Optical image of the single crystal of 1 (B) after laser irradiation. (E) Dark field image of c-HCSs placed onto fused silica. Scale bar, 3 µm.

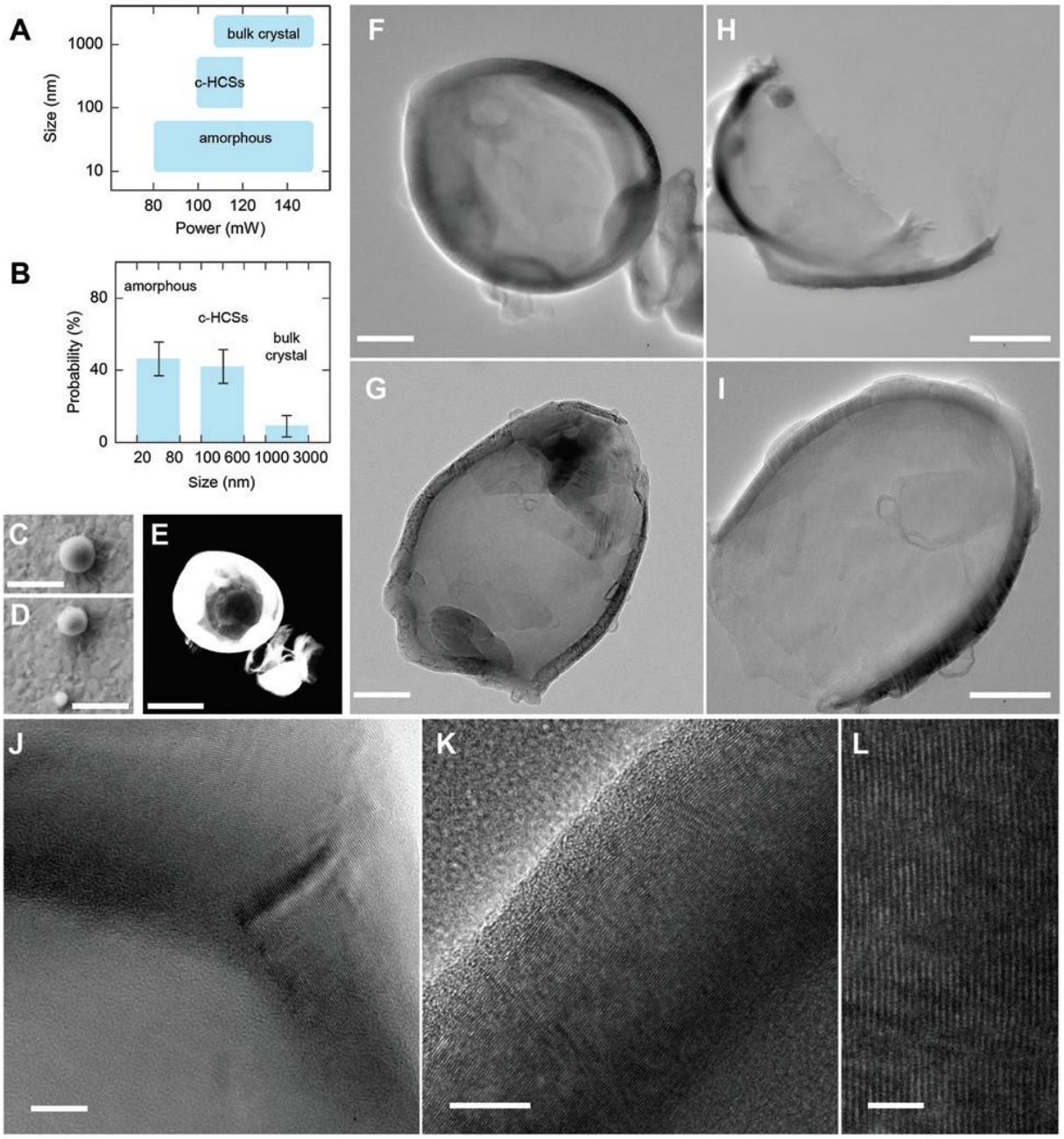

Fig. 2: The morphology of c-HCSs. (A and B) Statistical analysis of the products of the laser post treatment of MOF single crystals as a function of the laser power. The main products are amorphous 20–100 nm nanoparticles, small shards of MOFs and 100–600 nm crystalline hollow spheres and hemispheres with corresponding probability in (B) at a fixed laser power of 120 mW. (C and D) SEM micrographs of spherical c-HCSs onto a gold substrate. Scale bar, 0.5 µm. (E) Scanning TEM micrograph of spherical c-HCS demonstrating its hollow structure. Scale bar, 0.3 µm. (F and G) TEM micrographs of crystalline hollow spheres. Scale bar, 0.1 µm. (H and I) TEM micrographs of crystalline hollow hemispheres. Scale bar, 0.1 µm. (J to L) TEM micrographs of the crystalline shell of the spheres (F and G, respectively). Scale bar, 10 nm (J, K) and 2.5 nm (L).

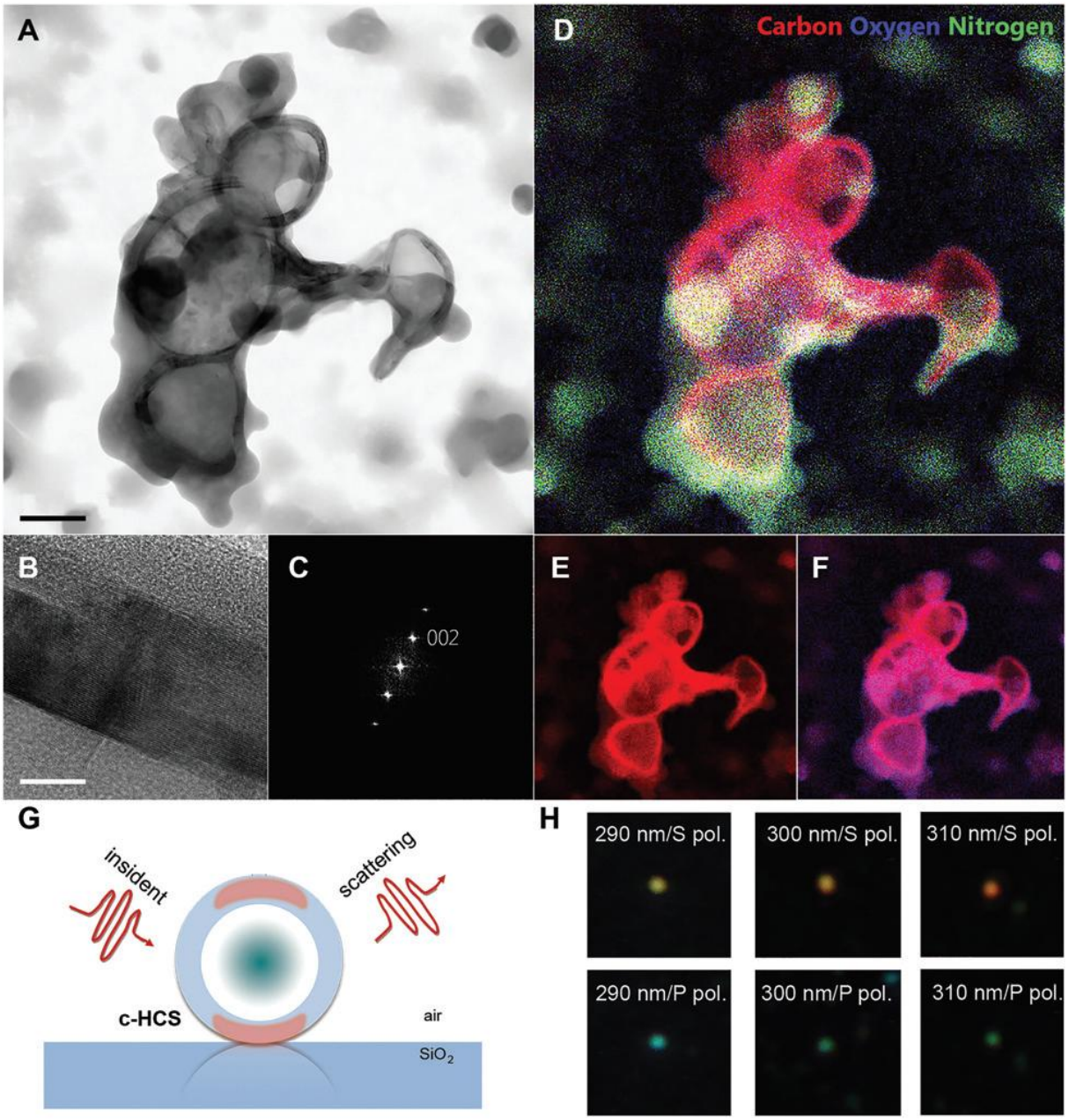

Fig. 3: The nature of c-HCS. (A) TEM micrograph of the spherical c-HCSs. Scale bar, 0.2 µm. (B, C) TEM micrograph of the shell of the c-HCS from (A) and its FFT spectrum providing the information about the interplanar distance dhkl (3.3 ± 0.1 Å). Scale bar, 10 nm. (D to F) EDX map of the corresponding c-HCSs. Red represents carbon, Blue represents oxygen, green represents nitrogen. (G) Schematic illustration of the scattering of light with S and P polarization by spherical c-HCS in dark field geometry. Red colour inside the shell illustrates the distribution of the electric field of magnetic Mie-type modes (ESI, Fig. S16), while the cyan cloud inside the cavity of c-HCS illustrates the localization of the magnetic part of light. (H) Dark field images of spherical c-HCS with different diameters (290 to 310 nm). The frequency of scattered light is determined by the polarization and c-HCS diameter.